JOURNAL OF SOLID STATE CHEMISTRY 117, 300–308 (1995)

A Family of One-Dimensional Oxides: Sr_3MIrO_6 (M = Ni, Cu, Zn): Structure and Magnetic Properties

T. N. Nguyen and H.-C. zur Loye[1]

Department of Chemistry, Massachusetts Institute of Technology, Cambridge, Massachusetts 02139

Received August 30, 1994; accepted November 10, 1994

The structures and magnetic properties of Sr_3ZnIrO_6, Sr_3CuIrO_6, and Sr_3NiIrO_6 are presented. The structure of Sr_3NiIrO_6 was solved by Rietveld analysis of powder neutron data. The structure refined in space group $R\bar{3}c$, with $a = 9.5806(1)$ and $c = 11.1315(2)$ Å. The structure consists of infinite chains of alternating IrO_6 octahedra and NiO_6 trigonal prisms. The structures of Sr_3ZnIrO_6 and Sr_3CuIrO_6 are closely related to that of Sr_3NiIrO_6. Magnetic susceptibility studies show that Sr_3NiIrO_6 undergoes complex magnetic transitions as a function of temperature and achieves a singlet ground state below 15 K. Low-temperature neutron diffraction does not show any evidence for structural changes. Magnetic susceptibility measurements of Sr_3CuIrO_6 display ferromagnetic ordering below 40 K. Measurements of the saturation magnetization at applied fields of up to 20 T display virtually no hysteresis loop, indicating that Sr_3CuIrO_6 is a very soft ferromagnet. The saturation magnetization of 0.61 μ_B is lower than that expected for two unpaired electrons. Sr_3ZnIrO_6 orders antiferromagnetically. The data were fit to an alternating-chain Heisenberg model. The structures and magnetic properties of these one-dimensional oxides are discussed.

INTRODUCTION

Low-dimensional materials, both one- and two-dimensional, have long been of interest to chemists and physicists because of their unique electronic and magnetic properties. The strong directionality of low-dimensional structures can produce highly anisotropic physical properties since interactions between electrons, such as magnetic coupling, can be strongly dependent on the crystallographic axes along which they occur. A wide variety of interesting properties have been observed in low-dimensional solids, including metal–insulator transitions (VO_2) (1), charge density waves (NbS_3) (2), superconductivity (Li_2NbO_2) (3), antiferromagnetism, and other more complex magnetic phenomena (4).

Magnetic systems of low dimensionality are of particular interest because they can exhibit a diversity of novel properties. For example, Haldane has discovered the existence of an energy gap between the nonmagnetic singlet ground state and the excited states for a Heisenberg one-dimensional antiferromagnet with integer spin (5, 6). In comparison, for a noninteger spin Heisenberg antiferromagnet, there is a continuum of excited states from the ground state without a gap (7). Haldane's theory, which predicts a singlet ground state, has been proven experimentally (8–10).

We recently reported on a new one-dimensional oxide, Sr_3NiPtO_6, which contains Ni(II) in an unusual trigonal prismatic coordination (11). The structure of Sr_3NiPtO_6 consists of infinite chains of alternating face-sharing PtO_6 octahedra and NiO_6 trigonal prisms. The chains are separated by strontium cations. The magnetic properties of Sr_3NiPtO_6 and the structurally related Sr_3CuPtO_6 were reported. Magnetic susceptibility studies of Sr_3NiPtO_6 indicated the presence of Ni(II) ions with large single-ion anisotropy; the onset of short-range antiferromagnetic ordering occurred at ~25 K. In contrast, Sr_3CuPtO_6 exhibits $S = 1/2$ Heisenberg linear chain antiferromagnetism.

The magnetic materials discussed in this paper are structural, but not magnetic, analogs of the platinum oxides described in our previous publication. Substitution of diamagnetic, low-spin octahedral platinum (IV), by low-spin octahedral iridium (IV) (d^5), places an element having one unpaired electron into the octahedral site. Thus, instead of having alternating magnetic and diamagnetic centers, as in the platinum oxides, the iridium compounds have an octahedral site with one unpaired electron alternating with trigonal prismatic sites containing zinc, copper, or nickel, having zero, one, or two unpaired electrons, respectively. In this way, the number of unpaired electrons on the trigonal prismatic site can be varied systematically and the consequent changes in the magnetic properties of the system examined. The additional interactions between the electrons on the trigonal prismatic site and the single unpaired electron on the octahedral site lead to the more complex magnetic behavior observed in the iridium analogs, compared to the platinum-containing systems.

[1] To whom correspondence should be addressed.

0022-4596/95 $12.00

In this paper we report the structures and magnetic properties of Sr_3NiIrO_6, Sr_3CuIrO_6, and Sr_3ZnIrO_6. The magnetic properties of Sr_3CuIrO_6, which was originally prepared and structurally characterized by Neubacher and Müller-Buschbaum (12) are included for completeness. No characterization of the physical properties had been previously reported.

EXPERIMENTAL

Polycrystalline samples of Sr_3NiIrO_6, Sr_3CuIrO_6, and Sr_3ZnIrO_6 were prepared via solid state reactions. Stoichiometric amounts of $SrCO_3$ (Cerac, 99.5%), Ir metal (Aesar or Engelhard, 99.9%) and the appropriate first-row transition metal oxide, NiO (Cerac, 99.995%), CuO (Cerac, 99.999%), and ZnO (Aldrich, 99.9%), were intimately mixed under acetone using an agate mortar and pestle and pressed into pellets. The pellets were placed on platinum foil in alumina boats during heating to prevent aluminum contamination. Heating the samples at 1150°C for 2 weeks with intermittent grindings yielded single-phase materials.

Powder samples were structurally characterized using a Rigaku RU300 X-ray diffractometer using Cu$K\alpha$ radiation, λ = 1.5405 Å. An X-ray powder diffraction step scan was collected from 5–105° 2Θ in steps of 0.01° 2Θ using a collection time of 5 sec/step. A Rietveld refinement of the powder X-ray diffraction data was performed using the refinement package GSAS (13). Powder neutron diffraction data were collected from 7–120° 2θ with a step interval of 0.05° at the NIST nuclear facility at Gaithersburg, Maryland. The neutron wavelength was 1.5390 Å. Rietveld refinement of the powder diffraction data was performed using the refinement package GSAS.

The oxygen content of the samples was determined by thermogravimetric analysis (TGA) using a Cahn TG121 system. Samples weighing approximately 50–100 mg were heated to 900°C under 5% H_2/95% N_2. The initial oxygen content was back-calculated from the measured weight loss. Heating oxygen deficient samples under pure oxygen to 550–700°C resulted in a weight gain associated with the complete oxidation of the compounds.

Magnetic measurements were obtained using a Quantum Design MPMS SQUID magnetometer at temperatures ranging from 2 to 300 K. All samples were fully oxidized by annealing under O_2 at 550–750°C before being used for any magnetic measurements. For data collection, all samples were cooled in zero field to 5 K. Once the sample temperature reached 5 K, the magnetic field was turned on and data were collected. All data were corrected for the diamagnetic contribution of the calibrated Kel-F sample container. High-field magnetic studies were performed at the Francis Bitter National Magnet Laboratory.

Electrical conductivity measurements were performed on sintered pellets using a Janis Research Co., Inc. conductivity apparatus equipped with a Keithley Model 236 electrometer and a Lakeshore 333 temperature controller. Gold wires were attached to the samples with conducting silver paint. Currents used were typically between 1 μA and 1 nA.

TABLE 1
Crystallographic Data for Sr_3NiIrO_6 at 298, 30, and 10 K

Formula	Sr_3NiIrO_6		
Formula weight	609.78		
Color	Black powder		
Space group	$R\bar{3}c$		
Z	6		
λ, Å	Neutron, 1.5390		
2θ scan range (°)	10–120		
Step interval (°)	0.05		
Maximum step intensity (counts)	2500		
Number of unique reflections	154		
Number of structural parameters[a]	10		
Number of background parameters	6		
Number of profile parameters	4		
Refinement	Rietveld using GSAS[b] with pseudo-Voight[c] peak shape functions		
	298 K	30 K	10 K
a (Å)	9.5806(1)	9.5783(1)	9.5783(1)
c (Å)	11.1315(2)	11.1323(2)	11.1321(2)
V (Å)	884.85(3)	884.48(3)	884.48(3)
R_{wp}[d]	6.23%	6.22%	6.28%
R_p[e]	4.99%	5.01%	4.96%
GOF (R_{wp}/R_e)	1.16	1.21	1.24
χ^2	1.35	1.36	1.43

[a] Includes atomic positional and displacement parameters and unit cell dimensions.

[b] A. C. Larson and R. B. von Dreele, General Structure Analysis System (GSAS), LANSCE, Los Alamos National Laboratory.

[c] P. Thompson, D. E. Cox, J. B. Hastings, *J. Appl. Cryst.* **20**, 79–83, (1987).

[d] $R_{wp} = [\Sigma\, w(I_o - I_c)^2/\Sigma\, wI_o^2]$.

[e] $R_p = \Sigma\,|I_o - I_c|/\Sigma\, I_o$, where I_o and I_c are the observed and calculated integrated intensities, respectively, and w is the weight derived from an error propagation scheme during the least-square refinement process.

RESULTS

Sr_3NiIrO_6

The structure of Sr_3NiIrO_6 was determined by Rietveld analysis of the powder neutron diffraction data using the program GSAS (see Table 1) and found to be isostructural with the platinum analog, Sr_3NiPtO_6. The powder samples of Sr_3NiIrO_6 were prepared by solid state reactions and had an oxygen stoichiometry of 5.9–6.0 as determined by thermogravimetric analysis. The oxygen content was a

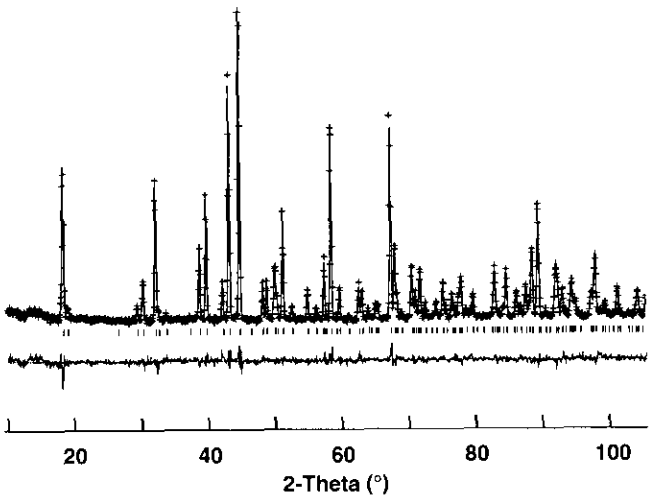

FIG. 1. Neutron Rietveld analysis for Sr_3NiIrO_6 at 298 K showing the observed, calculated, and difference patterns.

function of the cooling rate from high temperatures. Reactions in which the furnace was simply turned off at high temperatures gave the most oxygen deficient materials; however, the samples can be fully oxidized by annealing under oxygen at 550–750°C. Neutron diffraction data were collected on fully oxidized samples. The Rietveld refinement was carried out both in the space group of the platinum analog, Sr_3NiPtO_6, (11) $R\bar{3}c$, and in that of the structurally related Sr_3CuIrO_6, (12) $C2/c$. All attempts to refine the structure in the monoclinic space group diverged. Refinement of the Sr_3NiIrO_6 structure using the space group and atomic positions of Sr_3NiPtO_6 gave a unit cell of a = 9.5806(1) Å, c = 11.1315(2) Å and quickly converged to R_{wp} = 6.23%, R_p = 4.99%. The observed, calculated, and difference patterns are shown in Fig. 1.

Materials of composition Sr_3MIrO_6, M = Ni, Cu, Zn, have structures related to the one-dimensional structure of A_4PtO_6, where A = Ca, Sr, Ba. The A_4PtO_6 structure, space group $R\bar{3}c$, consists of infinite chains of alternating face-sharing PtO_6 octahedra and AO_6 trigonal prisms. In Sr_3NiIrO_6 the alkaline earth cation situated within the chains has been replaced by a first-row transition metal and the platinum has been replaced by the isovalent iridium. Consequently, the iridium and the nickel now alternate along the infinite chain. The structure of Sr_3NiIrO_6 is shown in Figs. 2 and 3. Figure 2 shows a single chain of Sr_3NiIrO_6 containing alternating Ni(II) in an unusual trigonal prismatic coordination and Ir(IV) in octahedral coordination. A view down the c-axis is shown in Fig. 3. The chains are separated by the strontium cations, which maintain charge balance and are located in square antiprismatic coordination. Table 2 lists the atomic positions and their estimated standard deviations, and selected bond distances and angles are displayed in Table 3.

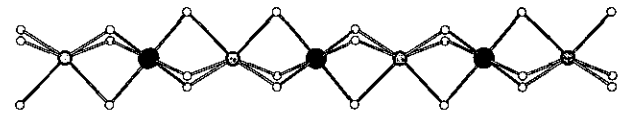

FIG. 2. A single chain in the Sr_3NiIrO_6 structure. Iridium, large shaded circles; nickel, small shaded circles; oxygen, open circles. The alternating IrO_6 and NiO_6 polyhedra have local O_h and D_{3h} site symmetry, respectively.

The Ni–O bond distance of 2.180(1) Å found for Sr_3NiIrO_6 is long; however, Ni(II)–O distances of up to 2.26 Å have been reported in La_2NiO_4 (1.95 and 2.26 Å) (14) and Y_2BaNiO_5 (1.88 and 2.19 Å) (10). The Ni–Ir distance of 2.7829(1) Å is somewhat short, but is still greater than the sum of the two atomic radii of 1.25 Å for Ni and 1.36 Å for Ir, ruling out direct metal–metal bonding. In the isostructural Sr_3NiPtO_6 compound (11) the d-bands are very narrow, suggesting the absence of Ni–Pt interactions and, furthermore, the crystal orbital overlap population (COOP analysis) also indicated no Pt–Ni bonding (15).

The magnetic susceptibilities of Sr_3NiIrO_6 at 3, 10, and 40 kG are shown in Fig. 4. The susceptibility is Curie-like from 300 to 150 K. Between 150 and 70 K there is a positive deviation from Curie-like behavior, followed by a large increase in the susceptibility starting at ~70 K and reaching a maximum susceptibility at T_{max} ~21 K. At temperatures below T_{max}, there is a precipitous drop in the magnetization to that of a constant singlet ground state for $T \leq 15$ K. The increase in the susceptibility below 70 K is especially sharp for the 3- and 10-kG data, but the 40-kG curve does not have a noticeable increase.

A plot of the effective moment, χT, as a function of temperature is shown in Fig. 5b. There are two peaks in the effective moment at ~90 and ~35 K followed by a

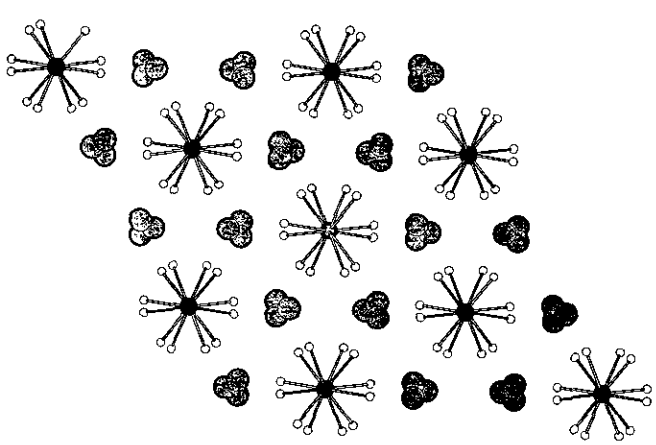

FIG. 3. The structure of Sr_3NiIrO_6 looking down the c-axis. Strontium, shaded circles; oxygen, open circles.

TABLE 2
Atomic Positions of Sr_3NiIrO_6 from Refinement of Neutron Data

Atom	x	y	z	Uiso ×100
		298 K		
Sr	0.3636(1)	0	1/4	0.45(3)
Ir	0	0	0	0.19(4)
Ni	0	0	1/4	0.76(5)
O	0.1732(1)	0.0230(1)	0.1134(1)	0.52(3)
		30 K		
Sr	0.3639(1)	0	1/4	0.11(3)
Ir	0	0	0	0.01(4)
Ni	0	0	1/4	0.09(4)
O	0.1737(1)	0.0232(1)	0.1136(1)	0.15(3)
		10 K		
Sr	0.3643(1)	0	1/4	0.12(3)
Ir	0	0	0	−0.10(4)
Ni	0	0	1/4	0.14(4)
O	0.1736(1)	0.0234(1)	0.1136(1)	0.16(3)

sharp decrease in the moment that converges to zero. These two maxima correspond to the positive deviation from Curie-like behavior between 150 and 70 K and the sharp increase in the susceptibility below 70 K, shown in the χ vs T plot (Fig. 5a). The sharp drop in the effective moment below 20 K is mirrored by the drop in the susceptibility below 21 K. The positive deviations are consistent with ferromagnetic interactions, while the decrease in the effective moment below 20 K indicates antiferromagnetic interactions.

To discover whether the abrupt drop in the susceptibility is caused by a structural transition at low temperatures, such as the dimerization of the magnetic nuclei along the chain, we performed low-temperature neutron diffraction

TABLE 3
Selected Bond Distances and Angles from Refinement of Neutron Data

	298 K	30 K	10 K
Ir–O (×6)	2.007(1)	2.012(1)	2.010(1)
Ir–Ni (×2)	2.78287(5)	2.78307(4)	2.78302(4)
Ni–O (×6)	2.180(1)	2.180(1)	2.179(1)
Sr–O (×2)	2.654(1)	2.654(1)	2.653(1)
Sr–O (×2)	2.468(2)	2.466(1)	2.470(1)
Sr–O (×2)	2.608(1)	2.606(1)	2.605(1)
Sr–O (×2)	2.733(2)	2.732(1)	2.730(2)
O–Ir–O (×6)	84.69(5)	84.67(5)	84.65(5)
O–Ir–O (×6)	95.31(5)	95.33(5)	95.35(5)
O–Ir–O (×3)	180	180	180

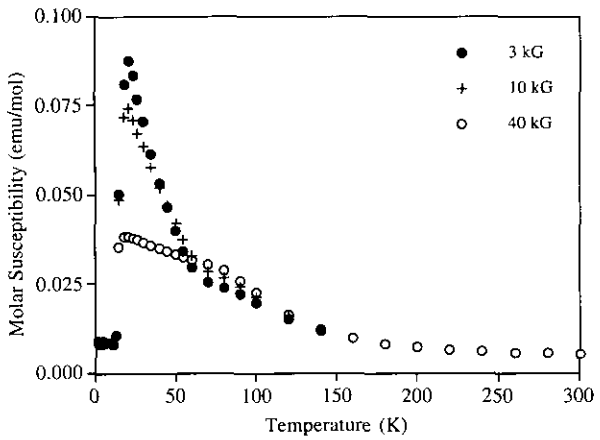

FIG. 4. Magnetic susceptibilities of Sr_3NiIrO_6 at 3, 10, and 40 kG.

studies at 10 K (singlet state region) and 30 K (ordering region). The data were refined in space group $R\bar{3}c$ using the refinement package GSAS, resulting in R_{wp} = 6.22%, R_p = 5.01% and R_{wp} = 6.28%, R_p = 4.96%, for the 30 K and 10 K data sets, respectively. The observed, calculated, and difference plots for the 30 and 10 K powder patterns are shown in Figs. 6 and 7, respectively, and the refinement data are shown in Table 1. With the exception

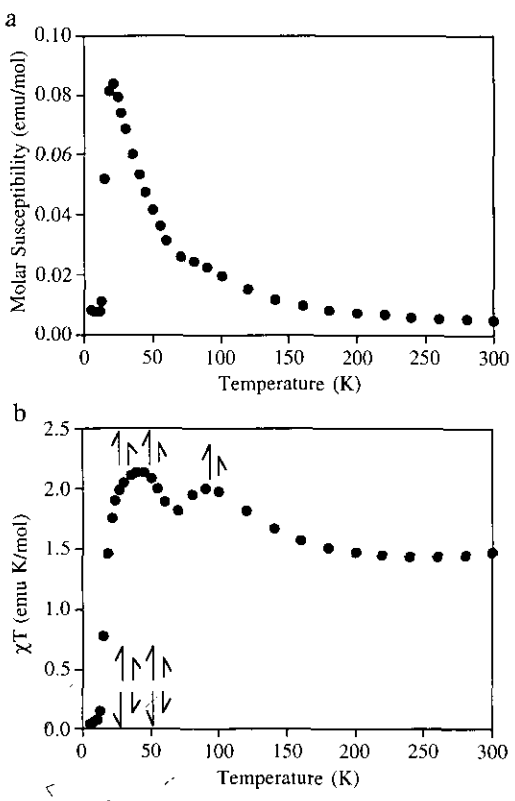

FIG. 5. (a) Magnetic susceptibility and (b) effective magnetic moment of Sr_3NiIrO_6 at 5 kG.

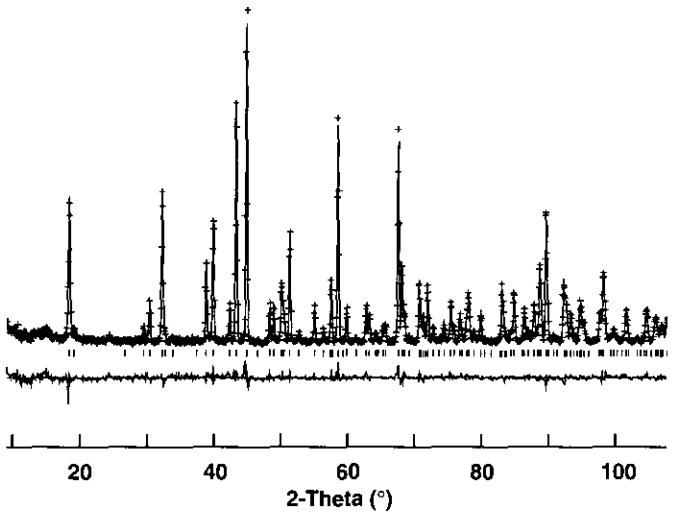

FIG. 6. Neutron Rietveld analysis for Sr_3NiIrO_6 at 30 K showing the observed, calculated, and difference patterns.

of the expected contraction in the unit cell parameters at lower temperatures, no structural changes were observed in the low-temperature studies. The atomic positions and their estimated standard deviations are listed in Table 2 and selected bond distances and angles are displayed in Table 3. No additional peaks suggesting the existence of a magnetic superstructure are observable.

Sr_3CuIrO_6

Both Sr_3CuIrO_6 and Ca_3CuIrO_6 have been structurally characterized by single-crystal X-ray diffraction (12, 16). Small single crystals of Sr_3CuIrO_6 and Ca_3CuIrO_6 were obtained by slow cooling the mixture of starting materials and by slow cooling in a CaF_2/KF flux, respectively. Sr_3CuIrO_6 can also be prepared by a solid state reaction of the simple oxides and iridium metal. Ca_3CuIrO_6, however, cannot be synthesized in such a manner. These materials are isostructural with Sr_3CuPtO_6 (17), containing alternating iridium oxygen octahedra and edge-shared copper oxygen square planes, rather than copper oxygen trigonal prisms. The square planar coordination is achieved by a displacement of the copper from the center into one of the rectangular faces of the trigonal prism.

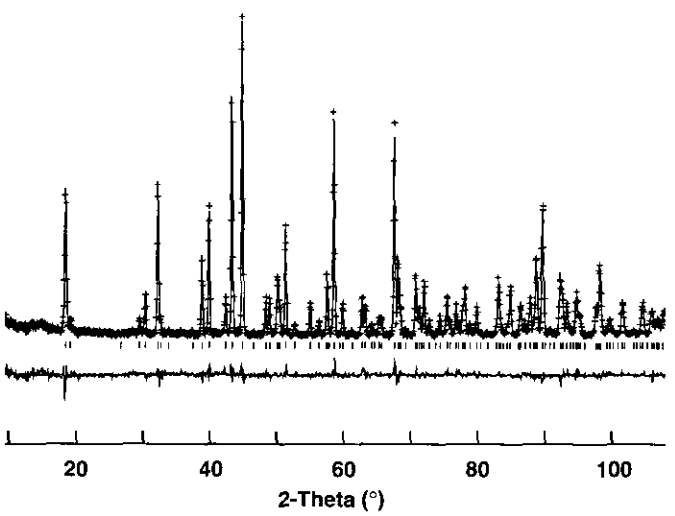

FIG. 7. Neutron Rietveld analysis for Sr_3NiIrO_6 at 10 K showing the observed, calculated, and difference patterns.

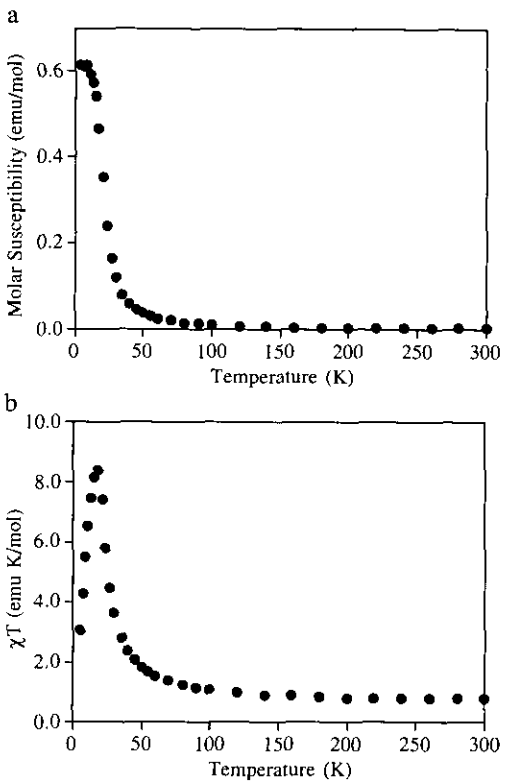

FIG. 8. (a) Magnetic susceptibility and (b) Effective magnetic moment of Sr_3CuIrO_6 at 5 kG. The χT curve indicates that the sudden increase in susceptibility at ~50 K is a ferromagnetic transition.

The magnetic susceptibility data of Sr_3CuIrO_6 are shown in Fig. 8a. The susceptibility is Curie-like between 300 and 40 K, followed by a large sharp increase at ~40 K, indicative of ferromagnetic ordering. Ferromagnetic ordering is also suggested by the χT plot shown in Fig. 8b. The effective moment is constant before the transition, as is expected for Curie-like behavior, and rises sharply upon reaching the ordering temperature. The moment then decreases at ~15 K because of magnetic saturation.

To further investigate the magnetic properties of this material, magnetic field dependence studies were performed. Figure 9a shows the field dependence of Sr_3CuIrO_6 at 5 K for positive and negative fields up to 4 T. The

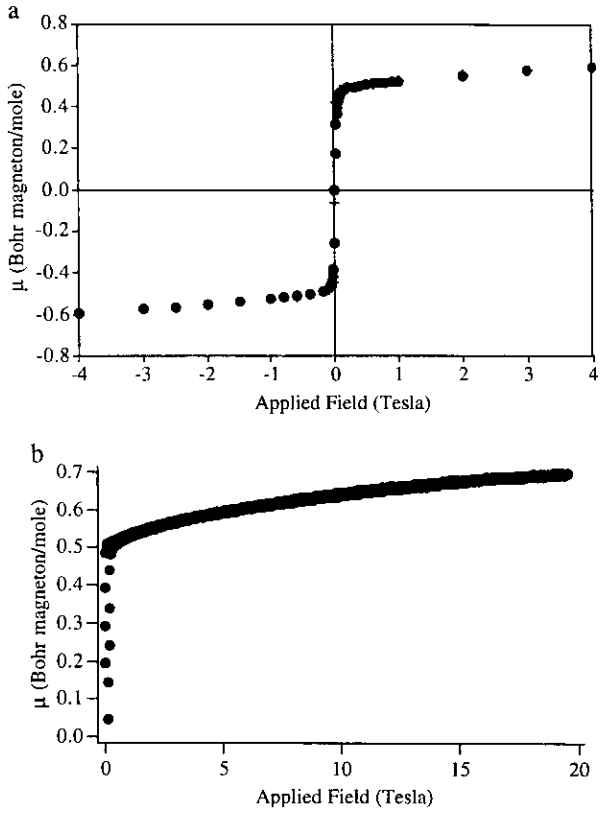

FIG. 9. (a) Field dependence of Sr_3CuIrO_6 at 5 K. Sr_3CuIrO_6 is a soft ferromagnet with a saturation magnetization of ~0.7 μ_B. (b) High-field dependence of Sr_3CuIrO_6 at 4.5 K.

magnetization loop is typical of a ferromagnet, and the noticeable lack of hysteresis suggests that Sr_3CuIrO_6 is an unusually soft ferromagnet. The experimentally found saturation magnetization is 0.61 μ_B per mole. High-field data were collected at Francis Bitter National Magnet Laboratory in a search for a second transition to a saturation magnetization corresponding to the 2 μ_B expected for a system containing two unpaired electrons. As is shown in Fig. 9b, at applied magnetic fields of up to 20 T, the saturation magnetization does not change appreciably from the low-field results.

The onset of magnetic ordering is also reflected in the electrical conductivity measurements performed on a sintered pellet of Sr_3CuIrO_6 (Fig. 10). At high temperatures, the noninteracting electrons are delocalized, and the conductivity is essentially constant, decreasing only slightly upon cooling. Upon reaching the ordering temperature, however, the conductivity decreases by a factor of approximately 4, indicating magnetic ordering and localization of the electrons.

Sr_3ZnIrO_6

The powder X-ray diffraction pattern of Sr_3ZnIrO_6 was indexed to a hexagonal unit cell of a = 9.6327(4) and c = 11.2022(5) Å. An attempt was made to refine the structure by Rietveld analysis of the powder X-ray diffraction data, using the structure of Sr_3NiIrO_6 as a starting point. The refinement converged to R_{wp} = 16% and R_p = 12.6%; however, the difference plot suggests that the structural model is incorrect. The structure was also refined in the monoclinic space group of Sr_3CuIrO_6, $C2/c$; however, no acceptable refinement was obtained for this space group either. Given the preference of Zn^{2+} for tetrahedral over trigonal prismatic coordination, it would not be surprising if Sr_3ZnIrO_6 were distorted from the Sr_3NiIrO_6 structure.

Sr_3ZnIrO_6 can be considered an analog of Sr_3CuPtO_6 with the spin located on the octahedral site rather than on the distorted trigonal prismatic site. In Sr_3CuPtO_6, there is one unpaired electron in the Cu(II) square planar site and no unpaired electron in the octahedral site occupied by the Pt(IV). Sr_3ZnIrO_6, on the other hand, contains no unpaired electron in the Zn(II), d^{10}, site, and the unpaired electron is now located in the octahedral site occupied by the Ir(IV), d^5.

One might expect that the magnetic properties of Sr_3ZnIrO_6 and Sr_3CuPtO_6 would be similar since they both have chains containing alternating spin one-half and spin zero. However, the different site symmetry of the unpaired electron in Sr_3ZnIrO_6—octahedral—versus that in Sr_3CuPtO_6—square planar—in addition to the different magnitudes of spin–orbit coupling for iridium versus copper leads to different magnetic behavior. Indeed, magnetic studies of Sr_3ZnIrO_6 at 5 kG (Fig. 11) reveal an antiferromagnetic transition at ~20 K, with a slightly different cusp shape than that observed for Sr_3CuPtO_6. The magnetic susceptibility data for Sr_3CuPtO_6 were successfully fit to a linear chain Heisenberg model (11). Attempts to fit the magnetic susceptibility data of Sr_3ZnIrO_6 to the same model resulted in poor fit. The fit, also shown in Fig. 11,

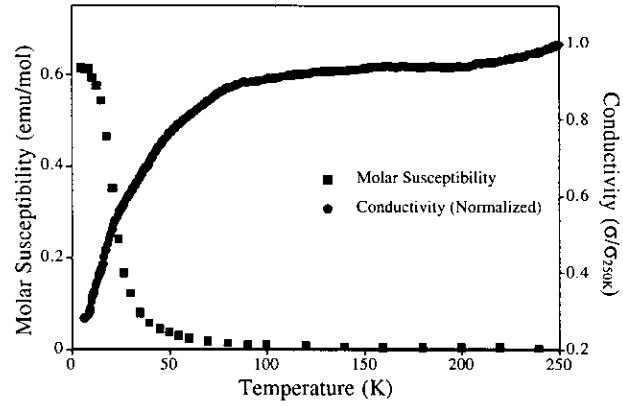

FIG. 10. Combined plot of the magnetic susceptiblity and the electrical conductivity of Sr_3CuIrO_6. The conductivity drops by a factor of 4 at approximately the temperature where ferromagnetic ordering sets in.

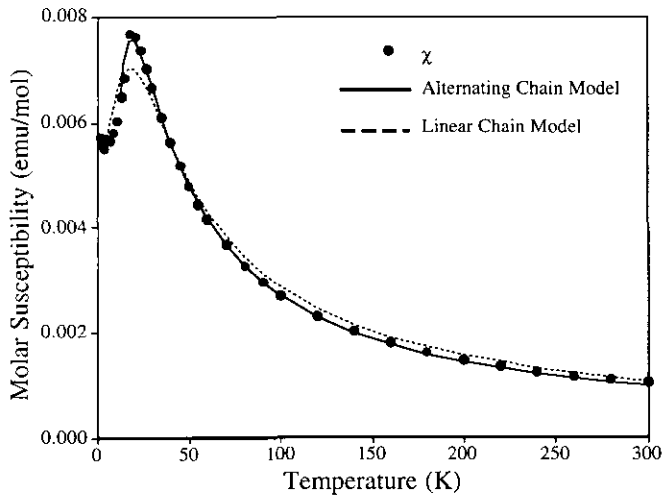

FIG. 11. Magnetic susceptibility of Sr_3ZnIrO_6 at 5 kG and best fits to the Heisenberg linear chain model and the alternating chain model.

predicted a broader transition and a lower susceptibility than were actually observed.

A good fit, however, was obtained by modeling the data using the alternating chain Heisenberg model (18–20). This model assumes that the magnetic exchange interaction between a magnetic ion and its nearest magnetic neighbor on one side is different from the magnetic exchange interaction with its nearest neighbor on the other side. In other words, there are two exchange constants, J, and they alternate along the chain. On the other hand, the linear chain Heisenberg model uses a Hamiltonian that accounts for nearest neighbor interactions isotropically, that is, the exchange between spins are all equivalent (21). The second exchange constant of the alternating chain model is generated by introduction of an alternation parameter, α, where $0 \leq \alpha \leq 1$(20). Thus, the Hamiltonian becomes

$$H = -2J \sum_{i=1}^{n/2} [\hat{S}_{2i} \cdot \hat{S}_{2i-1} \cdot \hat{S}_{2i+1}]$$

and the couplings along the chain alternate. When $\alpha = 1$, the model reduces to the linear chain model, and when $\alpha = 0$, the chain can be viewed as a series of dimers. The equation used to fit the data was obtained from Hatfield (22, 23). A least-square best fit gave $J/k = -15.6$ K, $g = 1.79$, and $\alpha = 0.11$. The small α value indicates that Sr_3ZnIrO_6 is magnetically more like a dimer than like a linear chain. The inequivalent magnetic exchanges predicted by the model imply that there should be alternating bond-length distances between the magnetic ions.

DISCUSSION

Trends in the Magnetic Data

The focus of this paper has been the structural and magnetic characterization of the one-dimensional oxides, Sr_3MIrO_6, where M = Zn, Cu, and Ni. As with the isostructural platinum-containing oxides, the ability of this structure to accommodate substitution on the trigonal prismatic M site allowed for the systematic study of the composition–magnetic property relationship in this series of materials. In the case of the iridium-containing oxides, however, the diamagnetic octahedral Pt(IV) site has been replaced by Ir(IV), which contains one unpaired electron.

As with the platinum-containing oxides, (11) the magnetic behavior of the iridium-containing oxides became more complex as the number of unpaired electrons on the M site was increased from zero to one to two. The structures of Sr_3NiIrO_6, Sr_3CuIrO_6, and Sr_3ZnIrO_6 are all related, yet differ in the exact coordination around the metal in the trigonal prismatic site. The nickel sits in the middle of the trigonal prismatic site, the copper is displaced into one of the faces, but the exact distortion for the zinc is not presently known. Given the preference of Zn^{2+} for tetrahedral coordination, however, we might expect a distortion that results in a tetrahedral-like environment for zinc.

Magnetically, the three compounds differ drastically. The magnetic susceptibility of Sr_3ZnIrO_6, a $S = 1/2$ system, displays antiferromagnetic ordering at 20 K and can be fit to an alternating chain model. Still, the exact nature of this magnetic behavior needs further study since the model requires alternating bond lengths between the magnetically coupled iridiums. The parent structure, Sr_3NiIrO_6, does not have alternating bond lengths. However, the Sr_3ZnIrO_6 structure appears to be distorted and consequently could give rise to alternating short and long bond lengths. Thus, given the magnetic data, we would expect the crystal structure to have two inequivalent Ir–Ir distances, which would lead at least to a doubling of the c-axis. Indexing of the Sr_3ZnIrO_6 X-ray diffraction data, however, results in lattice parameters that are almost identical to those of Sr_3NiIrO_6, suggesting that at room temperature there is no evidence of alternating bond distances. This fact does not eliminate the alternating chain model as a description of the magnetic behavior of Sr_3ZnIrO_6 at ~20 K: other materials with uniform distances between magnetic ions at room temperatures have been shown by dielectric measurements to undergo dimerization at lower temperatures (22, 23); the resulting phase transitions appear as anomalous peaks in capacitance measurements. Also, our X-ray diffraction data may not be sufficiently sensitive to detect possible oxygen position changes, and more sensitive methods, such as low-temperature neutron diffraction, might be necessary to reveal any structural deviations.

The replacement of diamagnetic Zn(II) with Cu(II),

which contains one unpaired electron, to form Sr_3CuIrO_6, creates a material that contains chains with two distinct $S = 1/2$ sites. These two sites order ferromagnetically, based on the magnetic susceptibility data shown in Figs. 8 and 9. It is worth pointing out that in these series of iridium-containing and platinum-containing oxides, Sr_3CuIrO_6 is the only material that contains only ferromagnetic coupling. This is interesting, especially since ferromagnetic ordering is rare in cuprates. The saturation magnetization of Sr_3CuIrO_6 is only 0.61 μ_B, lower than the expected 2 μ_B, the saturation moment for two unpaired electrons. Often an experimental saturation magnetization that is lower than expected can be explained by invoking ferrimagnetism or canted antiferromagnetism. In the case of ferrimagnetism, there are two sets of opposing, parallel spins with unequal magnitudes. The result is a net-spin with reduced magnitude. The ferrimagnetic model, however, is unlikely in the case of Sr_3CuIrO_6, since both copper and iridium have one unpaired electron each. In the case of a canted antiferromagnet, the spins are of equal magnitude, but they are not perfectly opposed as they would be in an ideal antiferromagnet. The net result is again a set of parallel spins with smaller magnitudes. This model, however, implies spin anisotropy, since the magnetic moments are not parallel.

Another model that can rationalize the experimental saturation magnetization is simple ferromagnetism that is not clearly manifested in the magnetic results. The observed saturation magnetization is 0.61 μ_B, or approximately one-third the expected saturation magnetization of 2 μ_B. Since the magnetic moment was measured on powder samples, the observed magnetization is the true magnetization averaged over the three crystallographic axes. Since the grains of material are randomly distributed, if two spin axes were statistically "locked in" space and unable to move and align with the applied field, then only one-third of the total magnetization would be observed. To verify this spin arrangement, a very large external field, up to 20 T, was applied in an attempt to align the spins physically. This field did not prove large enough to align the spins. Single crystal anisotropic magnetic measurements are needed to verify a ferromagnetic model. If this model is correct, a saturation magnetization of 2 μ_B will be observed in one crystallographic direction and no moment will be observed in the two perpendicular directions. Single crystal growth is in progress.

The substitution of Ni(II) for Cu(II) results in the compound Sr_3NiIrO_6, which contains chains with alternating $S = 1$ (Ni(II)) and $S = 1/2$ (Ir(IV)) centers. Sr_3NiIrO_6 displays the most complex magnetic behavior of all the platinum and iridium oxides in this series of one-dimensional compounds. The susceptibility curves shown in Fig. 4 are characteristic of an antiferromagnetic transition, and the decrease in susceptibilities at higher fields is indicative of spin saturation of ferromagnetic ordering. The two peaks in Fig. 5 indicate ferromagnetic interactions, while the decrease in moment indicates antiferromagnetic coupling. A possible explanation that describes the magnetic results is ferromagnetic exchange within the chains and antiferromagnetic exchange between the chains, giving a singlet ground state. At 90 K, the spins of Ni and Ir are aligning ferromagnetically within the chains, resulting in an increased magnetic moment. The larger increase in the magnetic moment at 35 K is due to additional Ni and Ir centers' coupling along the chains. At low temperatures, these chains, which contain intrachain ferromagnetic exchange, couple antiferromagnetically to give a zero effective moment.

TABLE 4
Summary of Magnetic Data

Sr_3NiIrO_6	Antiferromagnetism
Sr_3CuItO_6	Ferromagnetism
Sr_3ZnIrO_6	Antiferromagnetism
Sr_3NiPtO_6[a]	Antiferromagnetism
Sr_3CuPtO_6[a]	Antiferromagnetism
Sr_3CoPtO_6[b]	Random spin chain paramagnetism
Sr_3ZnPtO_6[b]	Diamagnetism
$Sr_3CuPt_{0.5}Ir_{0.5}O_6$[b]	Random spin chain paramagnetism

[a] T. N. Nguyen, D. M. Giaquinta, and H.-C. zur Loye, *Chem. Mater.* **6**, 1642 (1994).
[b] T. N. Nguyen, Thesis, Department of Chemistry, Massachusetts Institute of Technology, 1994.

It is interesting to note that the powder susceptibility of an antiferromagnet will normally converge to a value of two-thirds χ_{max}, the maximum susceptibility, after the ordering temperature (24). The magnetic transition to a singlet ground state, which occurs at ~21 K, might be explained by a structural transition such as dimerization of the magnetic nuclei within the chains. Low-temperature neutron data, however, provide no indication of either a structural transition or additional magnetic peaks that might arise from the dimerization of the magnetic centers along the chain.

As with the platinum-containing oxides, the iridium-containing oxides' magnetic behavior is altered by systematic substitutions. The addition of one unpaired electron to an otherwise diamagnetic site can have a significant effect on the magnetic properties of a material, as seen for Sr_3CuIrO_6, which is ferromagnetic, while Sr_3ZnIrO_6 is antiferromagnetic. The magnetic data for this family of one-dimensional compounds are summarized in Table 4. Even more interesting and complex magnetic behavior can be observed in solid solutions between the various members of this family. For example, random spin chain paramagnetism (25) is observed in $Sr_3CuPt_{0.5}Ir_{0.5}O_6$, on which we will report in the near future.

CONCLUSION

The magnetic properties of three one-dimensional oxides, Sr_3ZnIrO_6, Sr_3CuIrO_6, and Sr_3NiIrO_6, were discussed. These materials are the iridium analogs of the platinum oxide family, Sr_3MPtO_6, M = Ni, Cu, Zn. These structural analogs allow the investigation of the effects on the magnetic properties of this structural family when a diamagnetic transition metal in the chain is replaced with one that contains one unpaired electron. As expected, this exchange results in magnetic behavior of increasing complexity, where apparently the specific site symmetry of the magnetic centers has an important effect on the observed magnetic property. The magnetic susceptibility data of Sr_3ZnIrO_6 could be fit best to an alternating linear chain antiferromagnetic model. Sr_3CuIrO_6 was found to be a ferromagnet with a lower than expected saturation magnetization, and finally, Sr_3NiIrO_6, displays complex magnetism indicative of both intrachain ferromagnetic and interchain antiferromagnetic interactions.

ACKNOWLEDGMENTS

We thank J. Stallick for collecting the neutron data. This work was supported by the Massachusetts Institute of Technology, Center for Materials Science and Engineering under Grant DMR 9022933.

REFERENCES

1. F. J. Morin, *Phys. Rev. Lett.* **3,** 34 (1959).
2. J. Rouxel (Ed.), *in* "Physics and Chemistry of Materials with Low-Dimensional Structures" Vol. 2. pp. 1–26. Reidel, Boston, 1986.
3. M. J. Gesselbracht, T. J. Richardson, and A. M. Stacy, *Nature* **345,** 324 (1990).
4. R. L. Carlin, *in* "Magnetochemistry," p. 163. Springer-Verlag, Berlin, 1986.
5. F. D. M. Haldane, *Phys. Lett. A* **93,** 463 (1983).
6. F. D. M. Haldane, *Phys. Rev. Lett.* **50,** 1153 (1983).
7. J. des Cloiseaux and J. J. Pearson, *Phys. Rev.* **128,** 2131 (1962).
8. V. Gadet, *et al.*, *Phys. Rev. B* **44,** 705 (1991).
9. J. P. Renard *et al.*, *J. Appl. Phys.* **63,** 3538 (1988).
10. J. Darriet and L. P. Regnault, *Solid State Commun.* **86,** 409 (1993).
11. T. N. Nguyen, D. M. Giaquinta, and H.-C. zur Loye, *Chem. Mater.* **6,** 1642 (1994).
12. M. Neubacher and H. Muller-Buschbaum, *Z. Anorg. Allg. Chem.* **607,** 124 (1992).
13. A. C. Larson and R. B. vonDreele, General Structure Analysis System (GSAS), LANSCE, Los Alamos National Laboratory, Los Alamos, NM, 1990.
14. J. D. Jorgensen, B. Dabrowski, S. Pei, D. R. Richards, and D. G. Hinks, *Phys. Rev. B.* **40,** 2187 (1989).
15. G. Vajenine and R. Hoffmann, private communication.
16. A. Tomaszewska and H. Muller-Buschbaum, *Z. Anorg. Allg. Chem.* **619,** 534 (1993).
17. A. P. Wilkinson, A. K. Cheetham, W. Kunnman, and A. Kvick, *Eur. J. Solid State Inorg. Chem.* **28,** 453 (1991).
18. W. J. Duffy and K. P. Barr, *Phys. Rev.* **165,** 647 (1968).
19. K. M. Diederix, H. W. J. Blote, J. P. Groen, T. O. Klaassen, and N. J. Poulis, *Phys. Rev. B* **19,** 420 (1979).
20. J. C. Bonner, S. A. Friedberg, H. Kobayashi, D. L. Meier, and H. W. Blote, *Phys. Rev. B* **27,** 248 (1983).
21. J. C. Bonner and M. E. Fisher, *Phys. Rev.* **135,** 640 (1964).
22. J. W. Hall, W. E. Marsh, R. R. Weller, and W. E. Hatfield, *Inorg. Chem.* **20,** 1033 (1981).
23. W. E. Hatfield, *J. Appl. Phys.* **52,** 1985 (1981).
24. R. L. Carlin, "Magnetochemistry." Springer-Verlag, Berlin, 1986.
25. A. Furusaki, M. Sigrist, P. A. Lee, K. Tanaka, and N. Nagaosa, *Phys. Rev. Lett.*, **73,** 2622 (1994).
26. T. N. Nguyen, Thesis, Department of Chemistry, Massachusetts Institute of Technology, 1994.
27. P. Thompson, D. E. Cox, and J. B. Hastings, *J. Appl. Cryst.* **20,** 79–83 (1987).